Umklapp electron-electron scattering in bilayer graphene moiré superlattice

Christian Moulsdale [1,2,*] and Vladimir Fal'ko [1,2,3]

[1] *Department of Physics and Astronomy, University of Manchester, Manchester M13 9PL, United Kingdom*
[2] *National Graphene Institute, University of Manchester, Manchester M13 9PL, United Kingdom*
[3] *Henry Royce Institute, Institute for Advanced Materials, Manchester M13 9PL, United Kingdom*

(Received 1 November 2022; revised 6 April 2023; accepted 11 April 2023; published 25 April 2023)

Recent experimental advances have been marked by the observations of ballistic electron transport in moiré superlattices in highly aligned heterostructures of graphene and hexagonal boron nitride (hBN). Here, we predict that a high-quality graphene bilayer aligned with an hBN substrate features T^2-dependent resistivity caused by umklapp electron-electron (Uee) scattering from the moiré superlattice, that is, a momentum kick by Bragg scattering experienced by a pair of electrons. Substantial Uee scattering appears upon p doping of the bilayer above a characteristic threshold, and its contribution towards the resistivity grows rapidly with hole density, until it reaches a peak value, then falling off by an order of magnitude. This rapid, nonmonotonic dependence of resistivity, in the density range where the system is otherwise highly conductive, suggests the possibility of a nonconventional field-effect transistor operation. We also analyze the influence of an electrostatically induced interlayer asymmetry (and the associated band gap) in the bilayer and trigonal warping on the electron-electron umklapp scattering.

DOI: 10.1103/PhysRevB.107.144111

I. INTRODUCTION

Umklapp electron-electron (Uee) scattering is a fundamental process contributing towards the electrical resistivity of ultraclean metals. In this process, a pair of electrons interact via Coulomb repulsion and simultaneously transfer momentum $\hbar\boldsymbol{g}$ to the crystalline lattice, where $\boldsymbol{g}$ is a reciprocal lattice vector (Bragg vector) of this lattice. Taking into account this momentum kick, the wave vectors of the incoming ($\boldsymbol{k}_{1/2}$) and outgoing ($\boldsymbol{k}_{3/4}$) electron states satisfy the following condition:

$$\boldsymbol{k}_3 + \boldsymbol{k}_4 = \boldsymbol{k}_1 + \boldsymbol{k}_2 + \boldsymbol{g}. \tag{1}$$

When such a process relocates a pair of electrons across the Fermi surfaces, as illustrated in Fig. 1 (left-hand-side panel), the resulting two-electron backscattering generates resistivity, in contrast to "normal" Coulomb scattering, which conserves the total momentum of the pair. The Uee contribution towards the resistivity typically has a T^2 temperature dependence [1], but it is difficult to otherwise vary its strength in metals, where the electron density and a size of the Fermi surface are set by the material's chemistry, and the latter may not contain states that satisfy the condition in Eq. (1).

With the availability of long-period superlattices, such as moiré superlattices (mSLs) in incommensurate heterostructures of graphene [2–10] or twisted graphene bilayers [11–14], it becomes feasible to vary the electron density across the range where Uee processes can be switched on/off and then its strength substantially varied. In a monolayer graphene/hexagonal boron nitride (hBN) heterostructure, it has been observed that, above a well-defined threshold density (which depends on the twist angle between graphene and hBN crystals), the rate of mSL-Uee gradually increases with doping, becoming a dominant factor in the resistivity at room temperature [10,15]. As epitaxial graphene growth on hBN typically results in a high alignment and therefore the longest

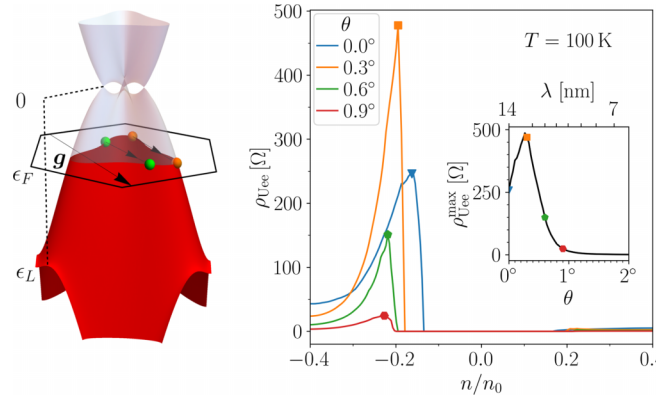

FIG. 1. Left: Umklapp electron-electron (Uee) scattering by a moiré superlattice in BLG. ϵ_F and ϵ_L are the Fermi energy and saddle point energy in the first mSL miniband on the valence side, respectively, counted from the conduction-valence band edge. Right: The nonmonotonic evolution of the contribution, $\rho_{\rm Uee} = T^2 f(n)$, of Uee scattering to the electrical resistivity against electron density n for various twists angles θ between graphene and hBN, at $T = 100$ K (Uee processes dominate when $T \ll |\epsilon_F|/k_B, |\epsilon_F - \epsilon_L|/k_B$). Inset: Peak value of the Uee resistivity, whose magnitude $\rho^{\rm max}_{\rm Uee}$ is shown as a function of the mSL period λ (and θ).

*christian.moulsdale@manchester.ac.uk

mSL periods [16–18], the Uee effect limits such scalable material utility in high-temperature electronics.

Here, we propose that, in contrast to monolayers, a peculiar dependence of the mSL-Uee resistivity in highly aligned bilayer graphene (BLG) on hBN has an opportunity for an unconventional field-effect transistor operation [19–21]. The Uee gives a contribution towards the resistivity,

$$\rho_{\rm Uee} \propto |n - n_*|^{1/2}|n|^{-2}T^2, \tag{2}$$

which features a rapid, nonmonotonic dependence on the electron density n shown in Fig. 1, and therefore a substantial transconductance in the doping region where the heterostructure would otherwise be highly conductive [22]. In particular, the Uee in BLG grows rapidly upon a threshold doping density n_*, then dropping down, which results in a prominent peak $\rho_{\rm Uee}^{\rm max}$ in the density-dependent resistivity. The size of this peak increases nonmonotonically with the mSL period λ (maximum value for $\lambda \approx 13$ nm) as a result of the interplay between the trigonal warping of the dispersion of electrons in BLG [23,24] and the mSL periodicity. To compare, in monolayer graphene the Uee resistivity increases monotonically with both density and mSL period [10,15], $\rho_{\rm Uee} \propto T^2|n - n_*|^{3/2}$ (due to the suppressed backscattering of Dirac electrons).

II. MODEL

The above predictions are derived by considering Uee scattering in the BLG/hBN heterostructure sketched in Fig. 2, enabled by the mSL at the graphene/hBN interface, whose period is determined by a $\delta = 1.8\%$ lattice mismatch between graphene and hBN and a misalignment angle θ. Projecting onto the low-energy bands of bilayer graphene in its $\boldsymbol{K}^\xi$ valley ($\xi = \pm$), the electronic properties of this system can be described by a 2×2 effective Hamiltonian [2,4,25,27]

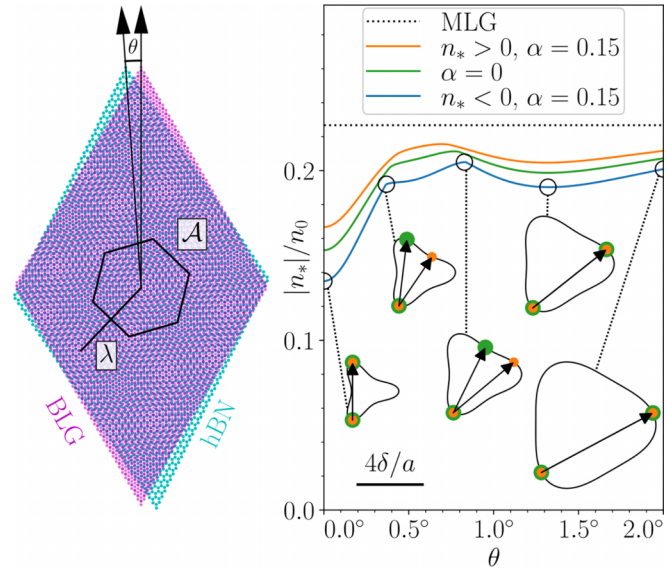

FIG. 2. Left: The lattice mismatch ($\delta \approx 1.8\%$) and twist θ between BLG and hBN gives rise to a moiré superlattice with period $\lambda \approx a/\sqrt{\delta^2 + \theta^2}$, and unit cell of area $\mathcal{A} = \sqrt{3}\lambda^2/2$. Right: The mSL-normalized magnitude $|n_*|/n_0$ ($n_0 = 4/\mathcal{A}$) of the threshold density of holes, $n_* < 0$, or electrons, $n_* > 0$, at which Uee scattering becomes possible due to a sufficiently large Fermi line. The threshold density n_* was calculated as a function of twist angle θ taking into account the particle-hole asymmetry in the BLG Hamiltonian ($\alpha = 0.15$), and compared to the symmetric cases of $\alpha = 0$ and the monolayer graphene superlattice ($|n_*| \approx 0.23\, n_0$).

$$\hat{H} = \frac{-1}{2m_*}\begin{pmatrix} 0 & \hat{\pi}^{\dagger 2} \\ \hat{\pi}^2 & 0 \end{pmatrix} + v_3\begin{pmatrix} 0 & \hat{\pi} \\ \hat{\pi}^\dagger & 0 \end{pmatrix} + \frac{\alpha\hat{\boldsymbol{p}}^2}{2m_*}\begin{pmatrix} 1 & 0 \\ 0 & 1 \end{pmatrix} - \frac{\Delta}{2}\left(1 - \frac{\hat{\boldsymbol{p}}^2}{m_*\gamma_1}\right)\begin{pmatrix} 1 & 0 \\ 0 & -1 \end{pmatrix} + \sum_{m=0}^{5}\hat{M}_{\boldsymbol{g}_m},$$

$$\hat{M}_{\boldsymbol{g}_m} = \begin{pmatrix} [u_0 + i(-1)^m u_3]e^{i\boldsymbol{g}_m\cdot\boldsymbol{r}} & \frac{1}{\sqrt{2m_*\gamma_1}}u_1(-1)^{m+1}e^{-i\xi m\pi/3}e^{i\boldsymbol{g}_m\cdot\boldsymbol{r}}\hat{\pi}^\dagger \\ \frac{1}{\sqrt{2m_*\gamma_1}}u_1(-1)^{m+1}e^{i\xi m\pi/3}\hat{\pi}\,e^{i\boldsymbol{g}_m\cdot\boldsymbol{r}} & \frac{1}{2m_*\gamma_1}[u_0 - i(-1)^m u_3]\hat{\pi}\,e^{i\boldsymbol{g}_m\cdot\boldsymbol{r}}\hat{\pi}^\dagger \end{pmatrix}, \tag{3}$$

where $\hat{\pi} = \hbar(-i\xi\partial_x + \partial_y)$ and $\hat{\boldsymbol{p}}^2 = -\hbar^2(\partial_x^2 + \partial_y^2)$. The first three terms are intrinsic to BLG, representing the effective electron mass, $m_* = \gamma_1/(2v^2) \approx 0.032\, m_e$, from the intralayer ($v$) and vertical interlayer (γ_1) couplings, trigonal warping from the skew interlayer (v_3) couplings [28], and a parabolic shift which lifts the particle-hole (ph) symmetry (α) [29], respectively. The fourth term represents an electrostatically controlled interlayer potential asymmetry Δ.

The final term in Eq. (3) represents the effects of the mSL sketched in Fig. 2, with harmonics corresponding to the first star of mSL Bragg vectors, $\boldsymbol{g}_m \approx \delta\cdot\boldsymbol{G}_m - \theta(\boldsymbol{e}_z \times \boldsymbol{G}_m)$ ($m = 0, 1, \ldots, 5$), where $\boldsymbol{G}_m = \frac{4\pi}{\sqrt{3}a}(-\sin\frac{m\pi}{3}, \cos\frac{m\pi}{3})$ is a graphene Bragg vector. This is parametrized by $u_{0/1/3}$, corresponding to an energy shift, gauge field, and mass term in the graphene layer closest to the hBN layer, respectively [30]. Each harmonic $\hat{M}_{\boldsymbol{g}_m}$ couples plane-wave states separated by $\boldsymbol{g}_m$, which reconstructs the conduction and valence bands of isolated BLG into minibands (see Fig. 1).

III. UMKLAPP ELECTRON-ELECTRON SCATTERING

For electrons on a superlattice, Coulomb interaction leads to mSL-Uee processes (see Fig. 1): Two electrons from one side of the Fermi line backscatter together to the other side, receiving a momentum kick ($\boldsymbol{g} = \boldsymbol{g}_m$) from the mSL. Such processes only occur when the size of the Fermi contour is sufficiently large compared to $|\boldsymbol{g}|$, giving a threshold electron density n_* which decreases with the size of the mSL unit cell. It is instructive to consider the "mSL-normalized" threshold n_*/n_0 (in the units of density, $n_0 = 4/\mathcal{A}$, of one filled spin-valley degenerate miniband), which dependence on the twist angle is shown in Fig. 2 for a gapless BLG ($\Delta = 0$). We find that, due to trigonal warping, n_*/n_0 increases with θ, which can be tracked to the Fermi contours at the Uee threshold

becoming less concave when $|n_*| > 2m^2 v_3^2/\pi$. The trigonal warping also pulls down the threshold density from the value $|n_*|/n_0 = \pi/(8\sqrt{3}) \approx 0.23$ established for the isotropic Dirac spectrum of monolayer graphene. Also, we analyze the effects of a conduction-valence band asymmetry in the bilayer dispersion, accounted for by the third term in Eq. (3) with $\alpha = 0.15$ [28]. The latter affects the concavity of the isoenergy lines, especially in the first valence miniband, making the threshold density $|n_*|$ slightly different for n and p doping of BLG mSL—see Fig. 2.

In the following, we derive the amplitudes for mSL-Uee processes, treating the mSL and electron-electron interactions in the lowest-order perturbation scheme. This is implemented for densities just above the threshold n_*, where the nonperturbative, resonant mixing of plane-wave states is negligible, which enables us to neglect the reconstruction of the electron dispersion into minibands. We account for the four leading Feynman diagrams involving Coulomb and mSL scattering of electrons off and back onto the Fermi level via an intermediate virtual state,

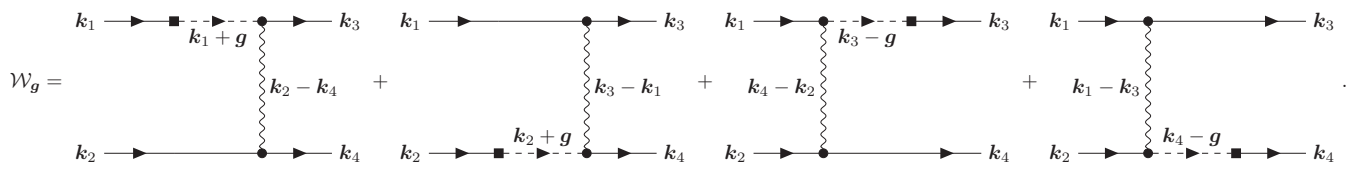

(4)

In each diagram, the initial and final momenta are related by Eq. (1); $\overset{q}{\bullet\!\sim\!\bullet} \equiv \tilde{V}(q) \approx W$ is the screened Coulomb interaction; $\blacksquare \equiv \hat{M}_g$ is an mSL interaction harmonic which imparts momentum kick $\hbar\boldsymbol{g}$; and $\overset{p}{\longrightarrow}$ is a propagator of an electron in the virtual state [31–35]. To mention, the mSL scattering amplitudes feature a particle-hole asymmetry, generic for graphene/hBN heterostructures, with values typically an order of magnitude larger in the valence miniband as compared to the conduction miniband [2–5].

IV. ELECTRONIC TRANSPORT

Equipped with the amplitudes in Eq. (4), we use linear transport theory [10,36,37] [see Supplemental Material (SM) [38]] to calculate the contribution of Uee processes to the resistivity,

$$\rho_{\rm Uee} = \frac{h}{6e^2}(k_B T)^2 \sum_{m=0}^{5} \int \frac{d\theta_1 d\theta_2}{|\boldsymbol{k}_3 \times \boldsymbol{k}_4|} \frac{k_1 k_2 k_3 k_4}{|v_{k1} v_{k2} v_{k3} v_{k4}|} |\mathcal{W}_{\boldsymbol{g}_m}|^2 v_{x1} \times (v_{x1} + v_{x2} - v_{x3} - v_{x4}) \Big/ \left(\int d\theta \frac{k}{|v_k|} v_x^2 \right)^2, \quad (5)$$

for $|n| \sim 10^{11}$ cm^{-2}. In this expression, $\boldsymbol{k}_i = k_i(\cos\theta_i, \sin\theta_i)$ is the wave vector of each electron ($i = 1, 2, 3, 4$) on the Fermi line, and $\boldsymbol{v}_i$ its group velocity. In Fig. 1, the results of this analysis are summarized for the vertically unbiased heterostructure, $\Delta = 0$. The Uee contribution is isotropic ($\rho^{\rm Uee}_{\alpha\beta} \equiv \rho_{\rm Uee}\delta_{\alpha\beta}$) due to the C_3 symmetry of the mSL. Also, note that the "normal" (momentum-conserving) electron-electron scattering suppresses higher-order harmonics in the nonequilibrium distribution of electrons, so that accounting for Uee becomes the same as accounting for an additional momentum transfer from the accelerated electrons (by the electric field) in the scattering time approximation (see SM [38]). Here, we limit the analysis of Uee to the density range of $0.1n_0 < |n| < 0.4n_0$, excluding from the analysis electron-hole scattering at the principal miniband edge and staying away from the mSL-induced van Hove singularity, where the perturbative treatment of the mSL interaction becomes inaccurate [39,40].

Typically, the Uee contribution in Eq. (5), $\rho_{\rm Uee} \approx T^2 f(n)$, rises rapidly above the threshold, $f(n) \propto |n - n_*|^{1/2}$. This singular behavior originates from the rapid expansion of

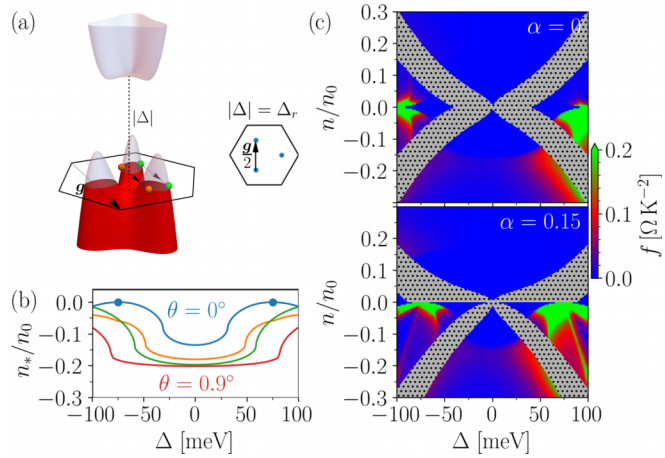

FIG. 3. (a) Umklapp electron-electron (Uee) scattering with momentum kick $\hbar\boldsymbol{g}$ between the three minivalleys in the valence miniband for nonzero interlayer potential asymmetry Δ opening a gap between the minibands. The minivalley edges are connected by $\boldsymbol{g}/2$ when this system is aligned (zero twist, $\theta = 0$) and $|\Delta| = \Delta_r$ (inset). (b) The nonmonotonic evolution of the valence miniband threshold density n_* with Δ for various twists, $\theta = 0°$–$0.9°$ from top to bottom, and $\alpha = 0.15$ ($n_* = 0$ when $\theta = 0$ and $|\Delta| = \Delta_r \approx 75$ meV). (c) The temperature-independent component f of the dominant contribution $\rho_{\rm Uee} \approx T^2 f$ of Uee processes to the electrical resistivity against electron density n, and Δ, with ($\alpha = 0$) and without ($\alpha = 0.15$) particle-hole symmetry, respectively. We exclude a (gray, dotted) butterfly-shaped region in each panel where the contributions of other processes are significant, whose wings are mirrored by zero layer polarization ($\Delta = 0$), and charge neutrality ($n = 0$) when $\alpha = 0$.

the phase space around the incoming/outgoing points in Fig. 2, with $\boldsymbol{k}_3 \times \boldsymbol{k}_4 = 0$ at the threshold. The exception is an initial interval of linear scaling, $f(n) \propto |n - n_*|$, found for the mSL with a twist angle in the range of $0.3^\circ < \theta < 0.8^\circ$. In both cases, the resistance subsequently falls off according to $|n|^{-2}$, as the approximately massive dispersion gives $\int d\theta k v_x^2/|v_k| \propto |n|$ in the denominator.

We also find that the interlayer potential asymmetry Δ, which opens a homogeneous band gap in BLG [41–44], has a pronounced effect on the Uee processes. The gap promotes the formation of three well-separated minivalleys at the BLG band edges, which persist up to the density $|n| \sim 2m|\Delta|^2/(\pi\gamma_1)$. The separation of the minivalleys increases with $|\Delta|$, thus decreasing the threshold doping density $|n_*|$ at which the Uee channel opens. For example, in the aligned BLG/hBN heterostructure ($\theta = 0$) with $|\Delta| = \Delta_r \approx 75\,\text{meV}$, the minivalleys are separated by the $\frac{1}{2}\boldsymbol{g}_m$, so that Uee scattering transfers pairs of electrons between these minivalleys even at small doping [corresponding to $n_* = 0$, as shown in Fig. 3(b)].

The results of numerical computations of the Uee resistivity contribution ρ_{Uee} across a broad range of parameters are summarized in Fig. 3(c). We highlight the regions where the resistivity is dominated by Uee processes, excluding a butterfly-shaped region where thermally activated electron-hole scattering processes may dominate. The wings of this butterfly, shown in the bottom panel, differ for n and p doping, which reflects the particle-hole asymmetry of the BLG dispersion (here, we use $\alpha = 0.15$ [29]), conversely being mirrored by charge neutrality ($n = 0$) for $\alpha = 0$ in the top panel. Regardless of α, the wings are mirrored by $\Delta = 0$, where the wave functions feature zero layer polarization. In contrast, the Uee contribution differs for positive and negative Δ. This is because the interlayer asymmetry gap (vertical bias) shifts the weight of the low-energy electron states towards/away from the bottom graphene layer, hence increasing/reducing the mSL scattering strength determined by the hBN crystal aligned with the BLG flake. Also, as in monolayer graphene mSL, Uee processes are much stronger for p doping (first miniband of holes) than for n doping, due to the particle-hole symmetry breaking by the mSL potential [2,10].

V. CONCLUSION

Overall, we predict a strong contribution of umklapp electron-electron scattering of moiré superlattice towards the resistivity of highly aligned BLG/hBN heterostrucutres, with a nonmonotonic density dependence near the Uee threshold. While the Uee role would increase at higher temperatures, at low densities (near the threshold) it will compete with

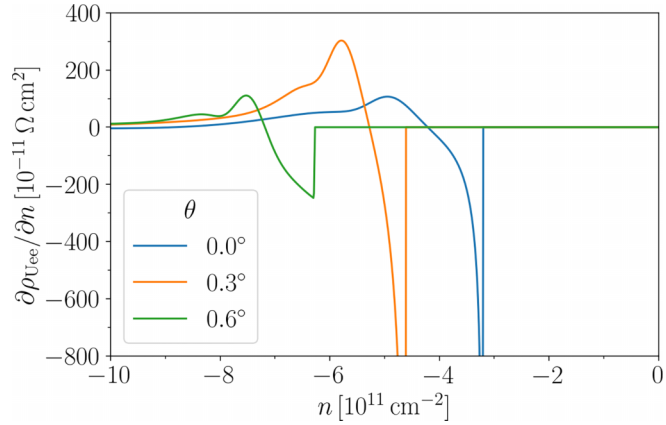

FIG. 4. For highly aligned BLG/hBN, a nonmonotonic dependence of Uee resistivity would produce a strong response to the gate voltage in the density range where the structure is highly conductive.

electron-hole scattering processes, promoted by electron-hole activation across the conduction-valence band edge [22]. Hence, for a more accurate description of the Coulomb scattering effect in the resistivity of mSL in bilayer graphene, one would need to account for both Uee and electron-hole scattering on equal footing. Also, one may want to extend the Uee analysis onto a broader range of miniband fillings, by calculating Uee rates using the full details of the mSL minibads spectra and Wannier functions, as attempted for a model graphene superlattice [45].

Finally, we note in Fig. 4 that the peak in the density dependence of the Uee resistivity in the nearly aligned BLG/hBN heterostructures, whose epitaxial growth has potential for scalable manufacturing [16–18], makes such a material suitable for an unconventional field-effect transistor operation [19–21]. Such a transistor can also be fast, as the predicted resistivity peak occurs at the carrier densities where such heterostructures are otherwise highly conductive (resistance under kΩ at room temperature [22]).

All the research data supporting this publication are directly available within this publication and Supplemental Material accompanying this publication [38].

ACKNOWLEDGMENTS

We thank A. Knothe, S. Slizovskiy, K. Novoselov, A. Geim, and R. K. Kumar for useful discussions. We acknowledge support from EU Graphene Flagship Project, EPSRC Grants No. EP/S019367/1, No. EP/P026850/1, and No. EP/N010345/1, and EPSRC CDT Graphene-NOWNANO EP/L01548X/1.

[1] A. H. MacDonald, R. Taylor, and D. J. W. Geldart, Phys. Rev. B **23**, 2718 (1981).
[2] J. R. Wallbank, A. A. Patel, M. Mucha-Kruczyński, A. K. Geim, and V. I. Fal'ko, Phys. Rev. B **87**, 245408 (2013).
[3] B. Hunt, J. D. Sanchez-Yamagishi, A. F. Young, M. Yankowitz, B. J. LeRoy, K. Watanabe, T. Taniguchi, P. Moon, M. Koshino, P. Jarillo-Herrero, and R. C. Ashoori, Science **340**, 1427 (2013).
[4] X. Chen, J. R. Wallbank, M. Mucha-Kruczyński, E. McCann, and V. I. Fal'ko, Phys. Rev. B **94**, 045442 (2016).
[5] M. Yankowitz, Q. Ma, P. Jarillo-Herrero, and B. J. LeRoy, Nat. Rev. Phys. **1**, 112 (2019).
[6] M. Yankowitz, J. Xue, D. Cormode, J. D. Sanchez-Yamagishi, K. Watanabe, T. Taniguchi, P. Jarillo-Herrero, P. Jacquod, and B. J. LeRoy, Nat. Phys. **8**, 382 (2012).

[7] C. R. Dean, L. Wang, P. Maher, C. Forsythe, F. Ghahari, Y. Gao, J. Katoch, M. Ishigami, P. Moon, M. Koshino, T. Taniguchi, K. Watanabe, K. L. Shepard, J. Hone, and P. Kim, Nature (London) **497**, 598 (2013).

[8] L. A. Ponomarenko, R. V. Gorbachev, G. L. Yu, D. C. Elias, R. Jalil, A. A. Patel, A. Mishchenko, A. S. Mayorov, C. R. Woods, J. R. Wallbank, M. Mucha-Kruczynski, B. A. Piot, M. Potemski, I. V. Grigorieva, K. S. Novoselov, F. Guinea, V. I. Fal'ko, and A. K. Geim, Nature (London) **497**, 594 (2013).

[9] R. K. Kumar, X. Chen, G. H. Auton, A. Mishchenko, D. A. Bandurin, S. V. Morozov, Y. Cao, E. Khestanova, M. B. Shalom, A. V. Kretinin, K. S. Novoselov, L. Eaves, I. V. Grigorieva, L. A. Ponomarenko, V. I. Fal'ko, and A. K. Geim, Science **357**, 181 (2017).

[10] J. R. Wallbank, R. Krishna Kumar, M. Holwill, Z. Wang, G. H. Auton, J. Birkbeck, A. Mishchenko, L. A. Ponomarenko, K. Watanabe, T. Taniguchi, K. S. Novoselov, I. L. Aleiner, A. K. Geim, and V. I. Fal'ko, Nat. Phys. **15**, 32 (2019).

[11] J. M. B. Lopes dos Santos, N. M. R. Peres, and A. H. Castro Neto, Phys. Rev. Lett. **99**, 256802 (2007).

[12] G. Li, A. Luican, J. M. B. Lopes dos Santos, A. H. Castro Neto, A. Reina, J. Kong, and E. Y. Andrei, Nat. Phys. **6**, 109 (2010).

[13] Y. Cao, V. Fatemi, A. Demir, S. Fang, S. L. Tomarken, J. Y. Luo, J. D. Sanchez-Yamagishi, K. Watanabe, T. Taniguchi, E. Kaxiras, R. C. Ashoori, and P. Jarillo-Herrero, Nature (London) **556**, 80 (2018).

[14] Y. Cao, V. Fatemi, S. Fang, K. Watanabe, T. Taniguchi, E. Kaxiras, and P. Jarillo-Herrero, Nature (London) **556**, 43 (2018).

[15] M. Kim, S. G. Xu, A. I. Berdyugin, A. Principi, S. Slizovskiy, N. Xin, P. Kumaravadivel, W. Kuang, M. Hamer, R. Krishna Kumar, R. V. Gorbachev, K. Watanabe, T. Taniguchi, I. V. Grigorieva, V. I. Fal'ko, M. Polini, and A. K. Geim, Nat. Commun. **11**, 2339 (2020).

[16] W. Yang, G. Chen, Z. Shi, C.-C. Liu, L. Zhang, G. Xie, M. Cheng, D. Wang, R. Yang, D. Shi, K. Watanabe, T. Taniguchi, Y. Yao, Y. Zhang, and G. Zhang, Nat. Mater. **12**, 792 (2013).

[17] A. Summerfield, A. Davies, T. S. Cheng, V. V. Korolkov, Y. Cho, C. J. Mellor, C. T. Foxon, A. N. Khlobystov, K. Watanabe, T. Taniguchi, L. Eaves, S. V. Novikov, and P. H. Beton, Sci. Rep. **6**, 22440 (2016).

[18] J. Thomas, J. Bradford, T. S. Cheng, A. Summerfield, J. Wrigley, C. J. Mellor, A. N. Khlobystov, C. T. Foxon, L. Eaves, S. V. Novikov, and P. H. Beton, 2D Mater. **7**, 035014 (2020).

[19] H. Wang, T. Taychatanapat, A. Hsu, K. Watanabe, T. Taniguchi, P. Jarillo-Herrero, and T. Palacios, IEEE Electron Device Lett. **32**, 1209 (2011).

[20] N. Petrone, T. Chari, I. Meric, L. Wang, K. L. Shepard, and J. Hone, ACS Nano **9**, 8953 (2015).

[21] N. Hasan, U. Kansakar, E. Sherer, M. A. DeCoster, and A. D. Radadia, ACS Omega **6**, 30281 (2021).

[22] C. Tan, D. Y. H. Ho, L. Wang, J. I. A. Li, I. Yudhistira, D. A. Rhodes, T. Taniguchi, K. Watanabe, K. Shepard, P. L. McEuen, C. R. Dean, S. Adam, and J. Hone, Sci. Adv. **8**, eabi8481 (2022).

[23] C. Gold, A. Knothe, A. Kurzmann, A. Garcia-Ruiz, K. Watanabe, T. Taniguchi, V. Fal'ko, K. Ensslin, and T. Ihn, Phys. Rev. Lett. **127**, 046801 (2021).

[24] A. Knothe and V. Fal'ko, Phys. Rev. B **98**, 155435 (2018).

[25] E. McCann and V. I. Fal'ko, Phys. Rev. Lett. **96**, 086805 (2006).

[26] E. McCann and M. Koshino, Rep. Prog. Phys. **76**, 056503 (2013).

[27] The full 4×4 Hamiltonian features two more bands at energies $\sim \pm\gamma_1$ which are projected onto the lower-energy bands using a Schrieffer-Wolff transformation [25].

[28] $v = 1.0 \times 10^6\ \mathrm{m.s^{-1}}$, $\gamma_1 = 0.381\ \mathrm{eV}$, and $v_3 = 1.2 \times 10^5\ \mathrm{m.s^{-1}}$ [25,26,46].

[29] $\alpha = 0.15$ due to the potential asymmetry between dimer and nondimer atoms, skew interlayer couplings, next-nearest-neighbor intralayer couplings, and nonorthogonality of atomic orbitals [25,26,46].

[30] $u_0 = 9\ \mathrm{meV}$, $u_1 = -17\ \mathrm{meV}$, and $u_3 = -15\ \mathrm{meV}$ [47].

[31] G. Borghi, M. Polini, R. Asgari, and A. H. MacDonald, Phys. Rev. B **80**, 241402(R) (2009).

[32] O. V. Gamayun, Phys. Rev. B **84**, 085112 (2011).

[33] S. Slizovskiy, A. Garcia-Ruiz, A. I. Berdyugin, N. Xin, T. Taniguchi, K. Watanabe, A. K. Geim, N. D. Drummond, and V. I. Fal'ko, Nano Lett. **21**, 6678 (2021).

[34] X. Liu, Z. Wang, K. Watanabe, T. Taniguchi, O. Vafek, and J. I. A. Li, Science **371**, 1261 (2021).

[35] We include the overlaps of the wave functions of the incoming and outgoing electrons with the operator at each vertex.

[36] J. M. Ziman, *Electrons and Phonons: The Theory of Transport Phenomena in Solids* (Oxford University Press, Oxford, UK, 1960), Chap. 9.14.

[37] L. D. Landau and E. M. Lifshitz, *Physical Kinetics*, Course of Theoretical Physics Vol. 10 (Pergamon Press, Oxford, UK, 1981), Chap. 79.

[38] See Supplemental Material at http://link.aps.org/supplemental/10.1103/PhysRevB.107.144111 for additional details on the scattering calculations in this paper.

[39] R. Hlubina, Phys. Rev. B **53**, 11344 (1996).

[40] Y. Xu, F. Herman, V. Granata, D. Destraz, L. Das, J. Vonka, S. Gerber, J. Spring, M. Gibert, A. Schilling, X. Zhang, S. Li, R. Fittipaldi, M. H. Fischer, A. Vecchione, and J. Chang, Commun. Phys. **4**, 1 (2021).

[41] K. F. Mak, C. H. Lui, J. Shan, and T. F. Heinz, Phys. Rev. Lett. **102**, 256405 (2009).

[42] Y. Zhang, T.-T. Tang, C. Girit, Z. Hao, M. C. Martin, A. Zettl, M. F. Crommie, Y. R. Shen, and F. Wang, Nature (London) **459**, 820 (2009).

[43] A. Ramasubramaniam, D. Naveh, and E. Towe, Nano Lett. **11**, 1070 (2011).

[44] W. Zhang, C.-T. Lin, K.-K. Liu, T. Tite, C.-Y. Su, C.-H. Chang, Y.-H. Lee, C.-W. Chu, K.-H. Wei, J.-L. Kuo, and L.-J. Li, ACS Nano **5**, 7517 (2011).

[45] H. Ishizuka and L. Levitov, New J. Phys. **24**, 052001 (2022).

[46] A. B. Kuzmenko, I. Crassee, D. van der Marel, P. Blake, and K. S. Novoselov, Phys. Rev. B **80**, 165406 (2009).

[47] M. Lee, J. R. Wallbank, P. Gallagher, K. Watanabe, T. Taniguchi, V. I. Fal'ko, and D. Goldhaber-Gordon, Science **353**, 1526 (2016).